Advanced Steel Construction – Vol. 15 No. 4 (2019) 386-397
DOI: 10.18057/IJASC.2019.15.4.9

STUDY OF SEISMIC RESISTANCE OF KIEWIT-8 DOME CONSIDERING KEY STRUCTURAL DESIGN PARAMETERS

Ming Zhang[1, *], Yao-Peng Liu[2], Zhi-Xiang Yu[1] and Gerry Parke[3]

[1] *School of Civil Engineering, Southwest Jiaotong University, Chengdu 610031, China (corresponding author)*
[2] *Department of Civil and Environmental Engineering, The Kong Kong Polytechnic University, Hong Kong, China*
[3] *Department of Civil and Environmental Engineering, University of Surrey, Guildford, Surrey GU2 7XH, UK*
** (Corresponding author: E-mail: zhangming@home.swjtu.edu.cn)*

ABSTRACT

A new seismic failure criterion is proposed for the Kiewit-8 (K8) dome subjected to earthquakes based on key structural parameters. Firstly, the K8 dome models were built in the finite-element package ANSYS after considering the key structural design parameters. Secondly, the incremental dynamic analysis was undertaken resulting in a typical structural damage index D_s. These were introduced to undertake the nonlinear dynamic response history analyses at each increased level of seismic records intensity and permitted the calculation of collapse loads of domes. Three hundred three-dimensional seismic records based on the main influential factors of ground motion were selected as input seismic waves. Thirdly, the lognormal distribution was selected to appraise collapse loads to gain the dynamic collapse fragility curves for domes after comparing three maximum likelihoods. Then, the lower bound collapse loads with 95% probability of non-exceedance changing with structural parameters were determined. Finally, relationships between lower bound collapse loads and five key structural parameters were separated out by using numerical matching methods, followed by a new seismic failure criterion for all the relationships including the five key structural parameters and a safety factor of 1.5. The new seismic failure criterion will contribute to the safe design and construction of these excellent space structures worldwide, particularly in the countries which are prone to earthquakes.

Copyright © 2019 by The Hong Kong Institute of Steel Construction. All rights reserved.

ARTICLE HISTORY

Received: 22 April 2019
Revised: 12 August 2019
Accepted: 15 August 2019

KEYWORDS

Domes;
New seismic failure criterion;
Collapse loads;
Key structural parameters;
95% probability of non-exceedance

1. Introduction

Single-layer domes are adopted worldwidely as long-span roofs in recent decades [1-3] because of their advantages, such as their good aesthetic appearance, large space coverage capability and sound structural performance. Current research work is mainly focused on the structural response [4-10], collapse [11-13] of the steel structure under different loads through experiment and numerical simulation analysis [14-18], considering stability and buckling [19-22]. Only few reports have investigated the structural dynamic failure modes [17, 19, 23, 24] and the seismic failure loads when the single-layer reticulated shells are subject to earthquakes. Especially in countries prone to earthquakes (or tremor), design methods considering not only static but also dynamic behavior are required. In the technical manual for designing and analyzing the space structures [25], the maximum displacement is restricted to 1/400 of the shortest span of the single-layer domes under the action of static loads and frequent tremors. But there are no design guidelines at present to deal with the design of single-layer domes subjected to severe tremors. Currently, the design process for single-layer domes under strong earthquakes are mainly referring to general steel structure guidelines and the engineer's experience [26-28]. In these circumstances, Zhi [23] empirically proposed two different criteria for predicting the failure loads of Kiewit-8 (K8) domes and cylindrical reticulated shells by determining the maximum nodal displacement and structural plastic deformation. However, the existing dynamic criteria need to be determined by undertaking a series of numerical analyses using finite element software, which is complicated and time consuming for the structural engineer. Therefore, there is a need to develop a systematic, practical and fast method to estimate the limit load of these shell structures.

In this paper, typical single-layer dome models of the K8 domes [23] were built in the finite-element package ANSYS [29]. This was undertaken after considering key structural factors, which have a great effect on the dynamic failure loads of these kind of structures. Secondly, an incremental dynamic analysis (IDA) [30] with a typical structural damage index D_s [23] were used to conduct nonlinear dynamic response history analyses (RHAs) at each increased level of seismic records intensity. This was used to determine the collapse loads of the domes whose failure modes were dynamic strength failure. For considering the action of the properties of earthquake waves on the failure loads, three hundred three-dimensional seismic records from the database of the COSMOS [31] on the basis of the main influential factors of ground motion, such as earthquake magnitude, distance, focal mechanism and site class, were selected as input seismic waves to obtain collapse fragility curves for the domes. Thirdly, the lognormal distribution [32] was selected to fit the collapse loads to obtain the collapse fragility curves for the domes under the action of seismic waves after comparing the results from lognormal, Weibull [33], and Gamma distributions [34, 35]. The lower bound collapse loads with 95% probability of non-exceedance [28, 36-38] changing with structural roof weights, spans, rise to span ratios and tube sections were determined based on the collapse fragility curves. Finally, relationships between the lower bound collapse loads and five key structural design parameters were separately selected out by numerical matching methods, followed by a new seismic failure criterion, a general equation, for all the relationships including the five key structural parameters and a safety factor of 1.5 [39]. The reason for the relatively higher safety factor is that the value of the statistical life [40-42] is significantly higher comparing with the cost of dome construction, which could increase the safety of the dome structures and reduce the risk of death.

2. Factors to be considered in the ultimate load evaluation and the dome models

2.1 Factors

The domes should be safely and properly designed not to buckle or collapse under design loads. The calculation of the critical load corresponding to the collapse stage under the action of earthquakes should consider several factors, such as membrane action, structural configuration, boundary conditions, materials, members, nodes, connections between members and nodes, geometric imperfections, load distribution, peak ground motion and the duration as well as the frequency of the ground motions. The following gives a short explanation of the key factors considered in the ultimate load evaluation.

The membrane action is the membrane stresses prevailing in the shell-like structures. The domes generally resist external loads through membrane action with relatively low bending moments, in a similar way to continuous shells. Accordingly, the K8 domes used in this paper were designed and modeled as thin shell-like forms. To comply with this assumption, the shape and boundary conditions should be compatible with the membrane action, leading to a state of small bending moments. In these types of thin structures, appropriate measures are required for avoiding shell-like collapse.

The support types greatly influence the behaviour of the domes. In general, the buckling failure load or collapse load is higher in the case of pin-support where the supports are fixed against translation but free for rotation, than in the case of simple-support where the supports are fixed against only vertical translation. The failure load is higher in the case of simple-support conditions than that in the case of free edges if the form and members are the same for each particular dome.

The members used in the reticulated shell were considered to be fabricated from high strength, ductile steel. The ultimate load should be evaluated taking into consideration the effects of Young's modulus, yield stress, and residual

stress in the fabricated members.

The members and nodes are the fundamental elements of domes. The member slenderness ratio, subtended half angle and the arrangement of members are regarded as the key factors for the ultimate load of the dome.

The connection between members mainly refers to the rigidity and strength provided at the connections. It is well known that when the bending stiffness at a connection is high enough, the ultimate loads can be increased on account of the full rigidity at the connection, while the ultimate load will be reduced if the joint rigidity is low.

Geometric imperfections are classified roughly into global geometrical imperfections associated with nodal deviations and member crookedness. In the case of the domes, the geometric imperfections should be considered when evaluating ultimate loads, and the magnitude of real imperfections should be as small as possible.

The load distribution includes uniform loads, asymmetric snow accumulation, and combined loads of uniform and concentrated areas over a local region.

The peak ground motion and the duration, as well as the frequency, are the three fundamental parameters of ground motions. All of them can change the ultimate load of the domes subjected to earthquakes.

2.2. Single-layer dome models

In view of the above factors, the K8 dome [23] and its classification, the members and the material of the members are presented in Figs 1a, b, c and d, respectively. The RHAs was carried out for the dome models with all the supports fixed against translation but free for rotation. The joints between the members were taken as rigid, which is in accordance with most of the constructed structures. The span L and rise f could control the shape of the dome. The PIPE20 [29] element was chosen to simulate the structural members which yield stress and Young's modulus are 235 MPa and 2.06×10^5 MPa, respectively. The bilinear isotropic hardening model for all of the elements was adopted. The roof weight including cladding is equivalent to the surface area supported and the lumped masses applied to the nodes are described by the point elements MASS21 [29]. The dead load distributions are all uniform loads for all domes selected in this paper. Rayleigh damping was assumed here, whose damping ratio was empirically set to be 0.02. The consistent mode imperfection method was adopted to consider the geometric imperfections referring to the technical manual [25], and the maximum value of the consistent mode was 1/300 of the span L. Other parameters of the selected domes were designed to meet the technical manual [25], such as tube slenderness ratio, subtended half angle and the arrangement of members. The basic configurations of the domes are listed in Table 1, other cases with changed parameters complying with the basic configurations, such as different uniform roof weight, spans, rise to span ratios and cross sections, are shown in Appendix Table 1.

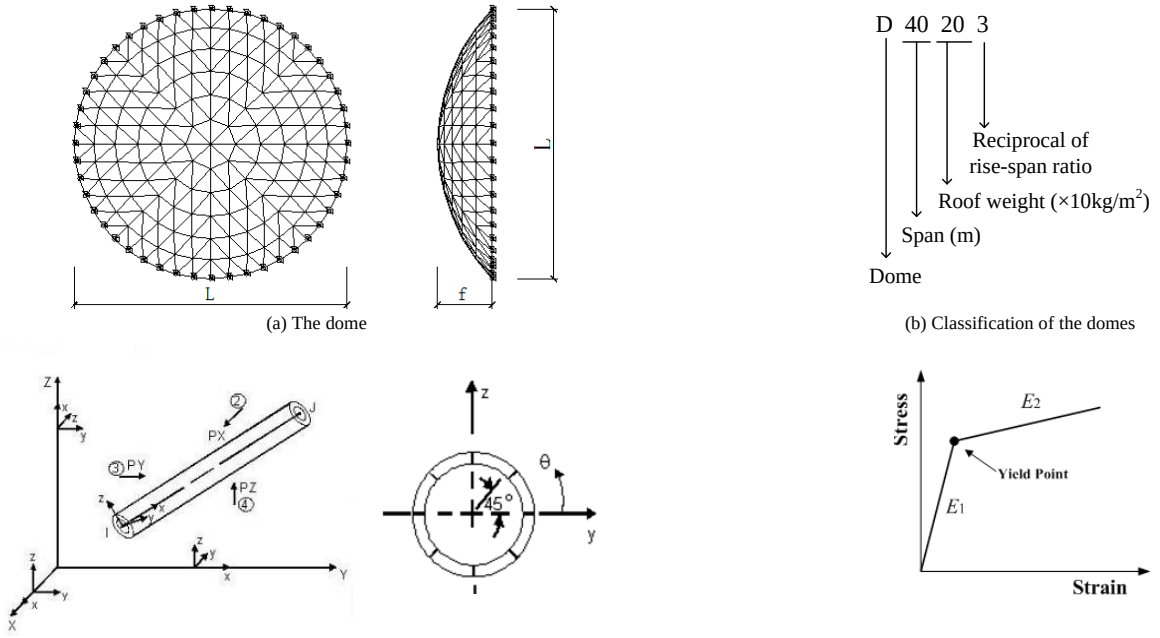

(a) The dome

(b) Classification of the domes

(c) The PIPE20 geometry [29]

(d) The material of the members

Fig. 1. The K8 dome system

The pipe20 [29] element can resist axial force, bending moment, shear, torque, etc. Meanwhile, the element has plastic, creep and swelling capabilities, and by using it, it is possible to output nodal displacements (including the nodal displacements in three directions at a node), member forces for nodes, shear strains, strain energy, and so on. In addition, there were eight integration points distributed uniformly around the cross-section of the pipe20 element presented in Fig.1c, which can output all the data information mentioned above.

Table 1

Labels and parameters of the K8 system

Dome label	Span (m)	Roof weight including cladding (kg/m²)	Rise to span ratio	Cross section (mm)	
				radial and hoop members	oblique members
D40203	40	200	1/3	146×5	140×6
D40205	40	200	1/5	146×5	140×6
D40207	40	200	1/7	146×5	140×6
D50063	50	60	1/3	168×6	152×5
D50065	50	60	1/5	168×6	152×5
D50067	50	60	1/7	168×6	152×5
D60063	60	60	1/3	194×6	168×6
D60065	60	60	1/5	194×6	168×6
D60067	60	60	1/7	194×6	168×6

3. The failure load (PGA), seismic records, and the lower bound failure load as well as its safety factor

3.1. The failure loads (PGA) of the domes

To obtain the collapse load of these structures, Ibarra and Krawinkler [43, 44] proposed using IDA method [30] to estimate the collapse load of the selected dome for each seismic record. Obtaining the dynamic collapse loads is a time-consuming job. In this study, the collapse states of the dome include dynamic instability and dynamic strength failure according to the definition of Zhi [23]. It is easy to judge the failure modes and failure loads for the dynamic instability as described in the literature [23]. However, it is difficult to discriminate its failure mode accurately for the dynamic strength failure because of the terrible plastic deformation and overall displacements before structures topple down. Here a failure criterion proposed in literature [23] is used to calculate failure loads of the domes whose failure modes are dynamic strength failure. The equation of the index D_s can be defined as:

$$D_s = 3.2\sqrt{(H/L)\left(100\left(\left(\frac{D-D_e}{L}\right)^2+\left(\frac{\varepsilon_a}{\varepsilon_u}\right)^2\right)+R_{1p}^2+R_{\beta p}^2} \quad (1)$$

where D_s is the structural damage index; H and L are the height and span of the dome, respectively; D refers to the nodal displacement, whose value is the largest comparing with other nodes in the selected dome; D_e accounts for the largest elastic displacement before entering plastic state; ε_a means the average strain for the global dome; ε_u equals the strain of steel when the failure occurred; R_{1p} and $R_{\beta p}$ are the plastic ratios of the members.

3.2. The seismic records

It is known to all that all the information contained in the seismic records, such as PGAs, durations and frequencies, can affect the structural dynamic response. In order to consider these factors as far as possible, three hundred seismic records from the database of the COSMOS [31] were selected as input seismic waves. In this paper, three hundred three-dimensional seismic records were selected from seven earthquakes on the basis of the main influential factors of ground motion mentioned above. The ratio of the PGAs along the three directions, X, Y and Z, was modulated into 1: 0.85 : 0.65 for all the seismic waves according to the technical manual [25], and the 90% energy duration T_d ($T_d = T_2 - T_1$, $\triangle E = E(T_2) - E(T_1) = 90\% E_a$, where E_a is the total energy) was adopted to calculate the durations of the input seismic waves.

3.3. Three probability distributions and the lower bound collapse load of the dome

Here, three hundred seismic records were selected to obtain the failure fragility curve based on three probability distributions, namely lognormal, Weibull and Gamma distributions, whose PDF and CDF are given by [32 - 35], presented in Eq. (2) – Eq. (8):

$$f_X(x) = \frac{1}{x\sigma\sqrt{2\pi}}\exp\left(-\frac{(\ln x-\mu)^2}{2\sigma^2}\right) \quad (2)$$

$$F_X(x) = \Phi\left(\frac{\ln x-\mu}{\sigma}\right) \quad (3)$$

$$f(x;\lambda,k) = \begin{cases}\frac{k}{\lambda}\left(\frac{x}{\lambda}\right)^{k-1}\exp\left(-\left(\frac{x}{\lambda}\right)^k\right) & x\geq 0\\ 0 & x<0\end{cases} \quad (4)$$

$$F(x;\lambda,k) = \begin{cases}1-\exp\left(-\left(\frac{x}{\lambda}\right)^k\right) & x\geq 0\\ 0 & x<0\end{cases} \quad (5)$$

$$f(x;k,\theta) = \frac{x^{k-1}e^{-\frac{x}{\theta}}}{\theta^k\Gamma(k)} \quad \text{for } x>0 \text{ and } k,\theta>0 \quad (7)$$

$$F(x;k,\theta) = \int_0^x f(u;k,\theta)du = \frac{\gamma\left(k,\frac{x}{\theta}\right)}{\Gamma(k)} \quad (8)$$

where $f_X(x)$ and $F_X(x)$ denote the PDF and CDF of the Lognormal distribution, X is the log-normally distributed random variable, x is the failure load PGA, μ and σ account for the mean value and standard deviation, Φ is the CDF of the standard normal distribution; $f(x; \lambda, k)$ and $F(x; \lambda, k)$ are the PDF and CDF of the Weibull distribution, $k > 0$ and $\lambda > 0$ refer to the shape parameter and the scale parameter; $f(x; k, \theta)$ and $F(x; k, \theta)$ equal the PDF and CDF of the Gamma distribution.

In addition, in this paper the Kolmogorov-Smirnov test [34, 35] was used to calculate the confidence level for the three probability distributions. It quantificationally analyzes the deviations between the hypothesized CDF $F_X(x)$ and the measured cumulative histogram, which can be given by

$$D = \max_{i=1}^{n}\left[\left|F^*\left(X^{(i)}\right)-F_X\left(X^{(i)}\right)\right|\right] = \max_{i=1}^{n}\left[\left|\frac{i}{n}-F_X\left(X^{(i)}\right)\right|\right] \quad (9)$$

where $X^{(i)}$ is the ith largest observed value in the random sample of size n.

After this, the PDF and CDF for the collapse loads of D40205 under the action of the three hundred ground motions are presented in Fig. 2 that have been fitted to the simulation results by lognormal, Weibull, and Gamma method. It can be seen from Fig. 2 that the lognormal distribution is the best fit to the dynamic failure loads and approximately satisfies the above test method with 95% confidence interval in agreement with these figures in Zhong's doctoral dissertation [45]. Hence, the lognormal distribution will be adopted to analyzing the dynamic failure fragility curves in this paper. The dome D40205 has a median dynamic failure load of 22.10m/s^2, whose logarithmic standard deviation is 0.2084. This dispersion only considered the uncertainty of ground motion, not included modeling uncertainty.

In practical engineering, a 95% probability of non-exceedance [28, 52, 36, 37] was the most commonly used to obtain a design value with credible and confidence intervals. In this paper the 95% confidence limit was also adopted to discriminate the lower bound collapse loads for domes subjected to the selected seismic records. In other words, the structural collapse loads for all the selected seismic waves would be larger than the lower bound collapse loads with 95% probability.

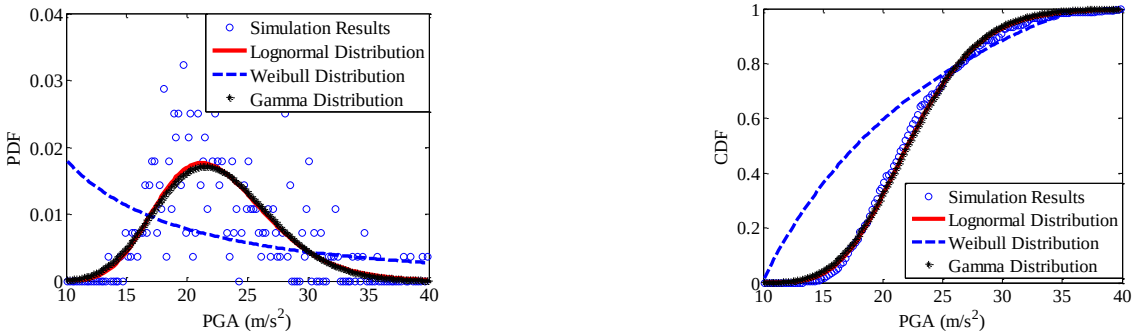

Fig. 2 The distributions for D40205 subjected to different seismic records

3.4. The safety factor and its rational

A dome should have sufficient capability to carry limit loads/design loads, as shown in Fig. 3, without large deformation detrimental to its serviceability state and load-bearing state. The ultimate load here is the load on the structure corresponding to ultimate point in Fig. 3, namely, corresponding to the collapse state. The ultimate loads of the domes can be calculated using FEA software. However, there is not a reasonable method to evaluate the limit loads/design loads for domes subjected to strong earthquakes at present. In the field of aircraft structures, the limit loads/design loads can be estimated by dividing the ultimate loads by, a factor of safety, 1.5, and the failure probability of the aircraft can be accepted. Because of the significance of domes, the same factor of uncertainty of 1.5 has been used to evaluate the limit loads/design loads, which can be obtained approximately using equation (10).

$$D_L = \frac{U_L}{1.5} \quad (10)$$

where the U_L is the ultimate loads and the D_L is the limit loads/design loads.

To confirm the rationality of the safety factor, the PGA-Displacement curve

for D40205 is shown in Fig. 3. In Fig. 3 the structural yield point denotes that the structure enters the plastic stage as shown in Fig. 4a; the design state (as shown in Fig. 4b) denotes the limit loads/design load and its corresponding displacement; and the ultimate point (as shown in Fig. 4c) denotes the structural maximum load and displacement followed by the structure collapse as shown in Fig. 4d.

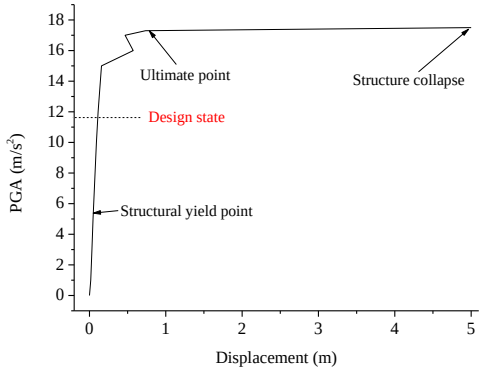

Fig. 3 The PGA-Displacement curve of D40205

As shown in Fig. 3, the PGA corresponding to the design state, of 11.53m/s^2, exceeds the PGA associated with the structural yield point, which indicates that the plastic yielding ability of the material has been partly used. Importantly, the displacement 0.11 m, nearly equals 1/400 of the structural span, and is less than 1/100 of the span of the domes which was proposed as the ultimate value of the critical displacement in reference [43] based on the statistical data and consideration of the practical factors related to design, construction, service, maintenance and restoration. In order to further verify the safety factor, Table 2 gives the collapse load, design load/limit load and ratio of the displacement corresponding to the design load/limit load to structure span for nine domes including D40205 under the action of the Taft wave recorded by station of USGS station 1095 in Kern County earthquake in 1952. In most cases the ratios of the displacement to the structural span are less than 1/100 as shown in Table 2. Only two of the nine displacements are a little larger than 1/100, but they are both very close to 1/100. These displacements can verify the sensibility of using a safety factor of 1.5, to a certain extent.

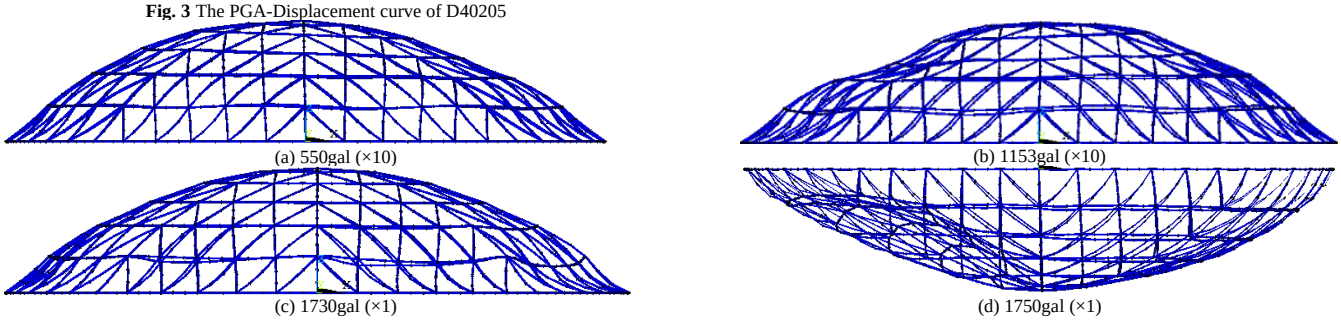

(a) 550gal (×10) (b) 1153gal (×10)

(c) 1730gal (×1) (d) 1750gal (×1)

Fig. 4 The deformation of D40205 subjected to the Taft wave at four critical stages.

Table 2
The dynamic failure stage of nine typical domes subjected to Taft wave

Dome	earthquake	Collapse load (m/s2)	Design load (m/s^2)	Displacement/span
D40203	Taft wave	12.00	8.00	0.93/400
D40205		17.30	11.53	1.00/400
D40207		16.50	11.00	3.42/400
D50203		43.00	28.67	1.41/400
D50065		64.50	43.00	2.95/400
D50207		57.30	38.20	4.58/400
D60063		48.30	32.20	2.67/400
D60065		64.30	42.87	3.15/400
D60067		52.70	35.13	4.44/400

Note: the Collapse load and Design load are the peak ground acceleration (m/s^2).

4. Relationship between the lower bound collapse load and key structural parameters

Table 3
Twenty seismic waves selected from the three hundred seismic records

Number	Stations	Number	Stations
1	CSMIP station 24272	11	CSMIP station 13879 Chino
2	CSMIP station 24401	12	MWD station 0709
3	CSMIP station 24399	13	CSMIP station 14828 Chino
4	CSMIP station 24207	14	CSMIP station 13095 Chino
5	CSMIP station 128	15	CSMIP station 23138 Chino
6	CSMIP station 24402	16	USGS station 0117
7	USC station 5361	17	TCU station 078
8	CSMIP station 23525 Chino	18	TCU station 116
9	USC station 0047	19	WNT station
10	CSMIP station 23842 Chino	20	USGS station 1095

Empirically, the ultimate loads of the domes have a close relation with the key structural factors like, dome spans, rise to span ratios, roof weights and member cross section sizes. Hence, numerical simulations for the ultimate loads of the domes with these key structural parameters mentioned above subjected to earthquakes were performed. To attain the collapse fragility curves of the ultimate loads and to reduce the computational effort, twenty seismic records with different frequencies and durations were selected as input seismic waves as shown in Table 3. Similarly, the IDA method was used to determine the collapse load for each seismic record. After this, the CDF distributions for the domes could be obtained based on the collapse loads, and the lower bound collapse load for each dome could be simultaneously discriminated with 95% probability. The relationships between each key structural parameter would then be analyzed independently, and an equation could be proposed to calculate the lower bound collapse load for the domes based on the five structural parameters. In this study, the prime target was to look for the relationship between the ultimate loads and the key structural parameters.

4.1. Relationship between lower bound collapse loads and roof weights

For buildings the relationship between the roof weights including cladding and the lower bound collapse loads, the RHAs were performed in the ANSYS software for a dome, whose span is 50 m and rise to span ratio is 1/5, with roof weights 60 kg/m^2, 100 kg/m^2, 160 kg/m^2, 200 kg/m^2, 260 kg/m^2, 300 kg/m^2, 360 kg/m^2, 400 kg/m^2 and 460 kg/m^2, which covered all cases in engineering applications [46], subjected to the twenty seismic records listed in Table 3. The collapse loads for the domes with different roof weights subjected to twenty seismic records are listed in Table 4, and their collapse fragility curves are presented in Fig. 5.

Table 4
The collapse loads for the domes with different roof weights subjected to twenty seismic records

Number	Collapse loads (m/s^2)								
	60 kg/m^2	100 kg/m^2	160 kg/m^2	200 kg/m^2	260 kg/m^2	300 kg/m^2	360 kg/m^2	400 kg/m^2	460 kg/m^2
1	120.60	76.00	39.00	27.40	17.00	11.80	6.00	5.20	3.00
2	100.50	58.60	31.00	20.60	14.00	9.60	6.40	5.20	2.80
3	136.80	79.60	42.80	31.40	18.20	13.40	8.00	5.60	3.00
4	138.80	86.60	46.00	29.80	22.00	14.00	9.00	7.20	4.00
5	97.40	64.00	35.80	25.60	17.20	12.60	7.60	5.60	3.00
6	124.60	76.80	44.60	31.00	19.40	12.80	9.00	5.80	3.80
7	118.20	35.80	42.40	31.20	19.80	15.00	9.20	6.80	4.00
8	92.40	59.80	35.80	25.60	16.80	13.00	7.80	5.60	3.20
9	61.40	36.00	18.00	12.00	7.00	4.80	3.20	2.40	1.20
10	111.80	73.80	43.60	30.80	19.60	14.40	8.40	6.40	3.40
11	105.60	66.80	41.40	31.40	20.40	14.60	8.80	6.40	3.40
12	123.80	88.80	44.00	30.00	23.00	15.00	10.80	8.40	3.40
13	159.40	95.80	49.80	32.40	19.40	15.60	10.40	7.20	4.40
14	133.80	82.00	51.60	35.00	19.80	14.00	7.40	5.80	3.20
15	118.60	79.80	47.00	32.00	21.60	16.00	10.40	8.20	4.60
16	70.80	42.60	23.60	16.40	9.20	6.60	4.00	3.20	1.60
17	65.40	35.40	18.40	12.60	7.60	5.20	3.60	2.80	1.40
18	55.40	31.60	16.40	12.00	7.00	5.00	3.40	2.40	1.40
19	88.60	52.60	29.80	21.40	13.80	10.40	6.60	5.00	2.80
20	64.50	38.00	20.40	13.40	8.20	5.60	3.20	2.80	1.80

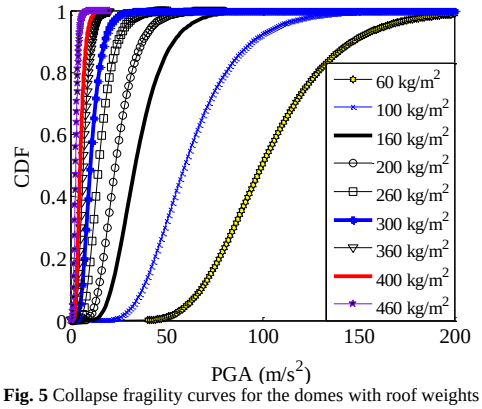

Fig. 5 Collapse fragility curves for the domes with roof weights

The lower bound collapse loads with 95% probability of non-exceedance changing with roof weights are given in Table 5 according to the failure fragility curves shown in Fig. 5.

On the basis of Table 5, the relationship between logarithmic lower bound collapse loads and roof weights are shown in Fig. 6. It demonstrates that there is a strongly statistically significant trend between logarithmic lower bound collapse loads (LPGA) and roof weights (RW) with a very small variance 0.12.

Empirically, the response variable *LPGA* can be written as a linear function of the predicator variable *RW* plus an error term. The linear prediction function has slope β and intercept α

$$\log(PGA)=\alpha+\beta RW+\varepsilon \quad (11)$$

where ε is an independent random variable, and its distribution has mean 0 and standard deviation σ.

Table 5
Lower bound collapse loads changing with roof weights

Dome	RW* (kg/m^2)	Lower bound Collapse load (m/s^2)
D50065	60	60.50
D50105	100	32.50
D50165	160	18.26
D50205	200	11.45
D50265	260	7.20
D50305	300	4.89
D50365	360	3.28
D50405	400	2.53
D50465	460	1.38

*Roof Weight

For these data, the least-squares method estimates of slope, intercept and error term were β=-0.009, α=4.4055 and σ=0.12, respectively. Therefore, the linear prediction function (11) can be rewritten as

$$\log(PGA) = -0.009RW + 4.4055 \pm 0.12 \quad (12)$$

where $RW \in$ [60 kg/m^2, 460 kg/m^2] is the roof weight including cladding.

4.2. Relationship between lower bound collapse loads and structural spans

In this section, the dome, whose roof weight is 60 kg/m^2 and rise to span ratio is 1/5, with spans 90 m, 85 m, 80 m, 75 m, 70 m, 65 m, 60 m, 50 m and 40 m were firstly selected as typical cases. Then the RHAs were performed in the ANSYS software for these typical cases subjected to the twenty seismic records listed in Table 3. The collapse loads for the domes with different spans subjected to twenty seismic records are listed in Table 6, and their collapse fragility curves, lognormal distributions, are shown in Fig. 7.

The lower bound collapse loads with 95% probability of non-exceedance changing with spans are then listed in Table 7 on the basis of the collapse fragility curves shown in Fig. 7.

On the basis of Table 7, the relationship between logarithmic lower bound collapse loads and spans is shown in Fig. 8. It demonstrates that there is also a strongly statistically significant trend between LPGA and spans with a very small variance 0.2788.

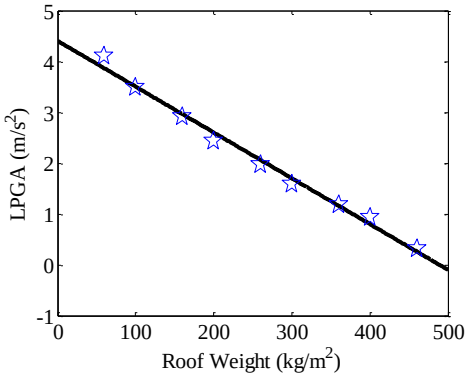

Fig. 6 Relationship between lower bound collapse loads and roof weights. (Note: the natural logarithm LPGA=log (Lower bound collapse load))

Table 6
The collapse loads for the domes with different spans subjected to twenty seismic records

Number	Collapse loads (m/s^2)								
	90 m	85 m	80 m	75 m	70 m	65 m	60 m	50 m	40 m
1	2.70	7.00	11.60	18.00	24.80	33.20	50.20	120.60	240.00
2	1.60	5.20	9.80	14.80	21.80	29.80	43.00	100.50	169.80
3	4.00	13.80	21.60	29.60	37.80	48.40	64.80	136.80	226.80
4	3.50	8.00	14.00	19.00	25.00	35.00	56.00	138.80	208.40
5	3.20	8.20	12.00	17.60	22.40	31.00	44.80	97.40	165.00
6	2.70	7.80	13.80	18.80	27.60	38.60	55.60	124.60	239.20
7	3.40	9.80	16.60	21.20	31.60	44.00	57.60	118.20	192.60
8	1.50	4.80	10.00	15.40	22.80	32.80	46.80	92.40	166.00
9	0.88	2.80	4.40	8.20	11.00	14.60	22.60	61.40	119.80
10	1.70	6.60	12.00	18.60	28.00	39.00	55.60	111.80	204.00
11	2.20	7.00	12.20	17.40	26.80	34.60	39.80	105.60	184.60
12	4.60	9.80	15.60	19.60	29.00	36.00	56.00	123.80	256.00
13	3.50	10.40	16.60	24.40	34.20	47.80	68.60	159.40	317.80
14	3.00	7.80	13.60	19.60	30.00	42.00	62.00	133.80	250.00
15	3.10	11.00	17.60	23.00	30.60	39.40	58.00	118.60	196.00
16	1.06	3.20	5.60	9.00	14.00	20.80	30.00	70.80	141.40
17	0.80	2.80	5.40	7.80	10.60	16.20	23.20	65.40	134.00
18	0.70	2.60	4.40	7.40	11.40	17.00	23.40	55.40	110.40
19	1.70	4.60	8.00	12.40	19.20	28.20	41.20	88.60	166.00
20	0.96	3.00	5.80	8.60	12.00	16.60	24.40	64.50	130.20

Table 7
Lower bound collapse loads changing with spans

Dome	Span (m)	Lower bound Collapse load (m/s2)
D90065	90	0.782
D85065	85	2.60
D80065	80	4.72
D75065	75	7.85
D70065	70	11.40
D65065	65	11.74
D60065	60	23.90
D50065	50	60.50
D40065	40	117.30

Referring to Equation (11), the relationship between lower bound collapse loads and spans could be given by:

$$\log(PGA) = -0.0923L + 8.6673 \pm 0.2788 \quad (13)$$

where $L \in$ [40m, 90m] is the structural span.

4.3 Relationship between lower bound collapse loads and rise to span ratios

Here, the domes, whose span is 50 m and roof weight is 60 kg/m^2, with rise to span ratios 0.10, 0.15, 0.20, 0.25, 0.30, 0.35, 0.40, 0.45 and 0.5 were firstly selected as typical cases. Then the RHAs were carried out in the ANSYS software for these typical cases subjected to the twenty seismic records listed in Table 3. The collapse loads for the domes with nine rise to span ratios subjected to twenty seismic records are given in Table 8, and their collapse fragility curves, lognormal distributions, are shown in Fig. 9.

The lower bound collapse loads with 95% probability of non-exceedance changing with rise to span ratios are presented in Table 9 based on the failure fragility curves shown in Fig. 9. Based on Table 9, the relationship between

logarithmic lower bound collapse loads and rise to span ratios is presented in Fig. 10. According to the LPGA changing to the cubic curve model is the best model among several different models of curve estimation with a very small variance 0.1122.

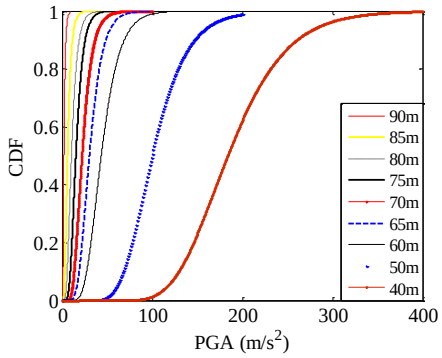

Fig. 7 Collapse fragility curves for the domes with different spans

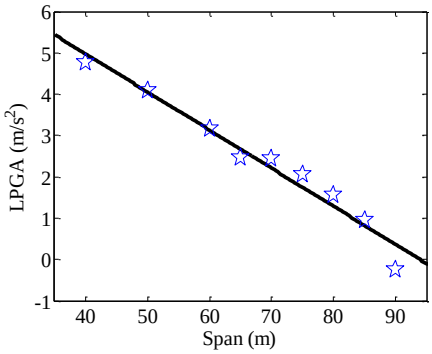

Fig. 8 Relationship between lower bound collapse loads and spans

Table 8
The collapse loads for the domes with nine rise to span ratios subjected to twenty seismic records

Number	Collapse loads (m/s^2)								
	0.10	0.15	0.20	0.25	0.30	0.35	0.40	0.45	0.5
1	73.00	115.60	120.60	123.00	112.20	110.10	118.80	96.60	83.60
2	64.20	94.40	100.50	36.60	66.00	75.00	87.60	73.40	58.80
3	106.80	99.80	136.80	140.80	94.40	49.80	103.80	104.00	118.20
4	97.60	125.80	138.80	116.00	105.80	91.80	78.80	71.60	68.80
5	68.40	94.40	97.40	118.40	119.00	87.60	150.20	99.80	97.80
6	99.40	119.80	124.60	153.60	130.20	129.40	152.40	127.40	113.00
7	94.00	108.80	118.20	115.80	155.40	153.60	170.00	140.20	123.20
8	72.20	94.80	92.40	79.00	69.60	63.40	55.60	49.00	42.00
9	36.60	54.60	61.40	48.40	41.80	39.40	42.60	30.60	26.20
10	78.60	117.00	111.80	100.60	90.60	86.40	82.20	69.20	57.40
11	94.60	112.60	105.60	93.60	86.00	87.40	90.80	83.40	74.00
12	102.00	128.00	123.80	119.20	122.20	130.60	201.60	156.60	140.40
13	123.60	155.80	159.40	158.60	139.80	136.80	149.00	116.40	105.00
14	106.60	144.00	133.80	136.60	166.00	158.20	140.20	127.40	107.60
15	88.80	117.00	118.60	114.00	108.00	108.60	103.00	90.60	78.80
16	57.40	77.60	70.80	52.00	45.00	41.00	37.80	31.00	24.90
17	36.80	56.20	65.40	54.80	49.00	43.80	49.60		31.40
18	29.00	54.40	55.40	42.20	34.60	28.00	21.80	17.60	14.00
19	45.20	81.20	88.60	83.00	76.00	68.80	66.60	52.80	46.20
20	40.40	60.00	64.50	50.20	48.60	42.40	47.20	32.60	26.80

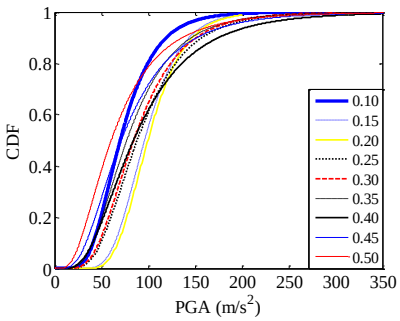

Fig. 9 Collapse fragility curves of the domes with different rise to span ratios

Table. 9
Lower bound collapse loads changing with rise to span ratios

Ratio	Lower bound Collapse load (m/s^2)
0.10	35.35
0.15	57.20
0.20	60.50
0.25	41.88
0.30	40.00
0.35	33.92
0.40	32.93
0.45	26.94
0.50	21.25

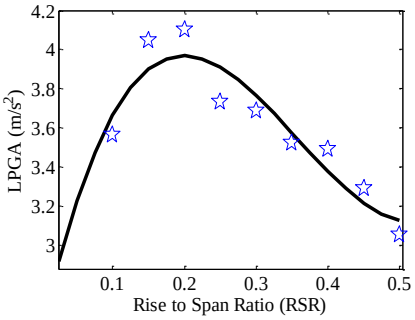

Fig. 10 Relationship between lower bound collapse loads and rise to span ratio

Referring to Equation (11), the relationship between the lower bound collapse loads and rise to span ratios could be given by:

$$\log(PGA) = 53.5354RSR^3 - 57.3447RSR^2 + 16.4657RSR + 2.5404 \pm 0.1122 \quad (14)$$

where $RSR \in [0.1, 0.5]$ is the rise to span ratio.

4.4 Relationship between lower bound collapse loads and tube member thicknesses

In this section, the dome spans D50065 with tube member thicknesses A, B, C, D, E and F were firstly selected as typical cases as shown in Table 11. Then the RHAs were performed in ANSYS software for these typical cases subjected to the twenty seismic records listed in Table 3. The collapse loads for D50065 with different tube thicknesses subjected to twenty seismic records are listed in Table 10, and their failure fragility curves, lognormal distributions, are shown in Fig. 11.

Table 10
The collapse loads for D50065 with different tube thicknesses subjected to twenty seismic records

Number	Collapse loads (m/s²)					
	A	B	C	D	E	F
1	106.00	120.60	127.20	150.40	162.80	149.80
2	86.00	100.50	103.60	121.20	119.60	135.60
3	118.00	136.80	146.00	159.80	220.00	215.80
4	117.20	138.80	140.00	160.20	164.00	149.60
5	86.60	97.40	99.20	122.00	119.80	144.60
6	107.60	124.60	126.60	152.40	171.60	186.80
7	101.20	118.20	120.00		156.60	166.20
8	81.00	92.40	93.40	109.40	114.40	128.00
9	50.40	61.40	62.40	76.60	74.60	84.80
10	96.80	111.80	113.00	133.20	141.20	157.80
11	87.20	105.60	106.60	123.40	130.60	144.40
12	104.60	123.80	124.60		154.60	169.60
13	131.60	159.40	159.80	192.60	212.80	243.60
14	112.60	133.80	136.00	159.60	177.60	196.20
15	104.60	118.60	121.00		147.00	163.00
16	58.60	70.80	71.80	85.60	85.20	96.80
17	53.60	65.40	66.40	79.40	77.60	89.60
18	46.40	55.40	56.40	68.00	70.20	80.40
19	77.20	88.60	90.00	105.00	119.60	133.20
20	54.80	64.50	65.60	80.40	81.80	

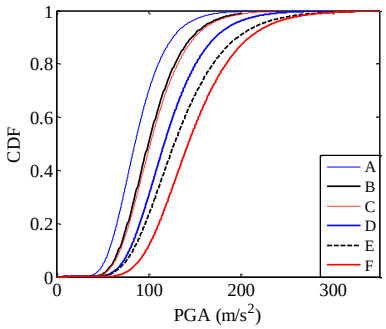

Fig. 11 Collapse fragility curves for D50065 with different tube thicknesses

The lower bound collapse loads with 95% probability of non-exceedance changing with tube thicknesses are presented in Table 11 on the basis of the failure fragility curves given in Fig. 11. Based on Table 11, the relationship between logarithmic lower bound collapse loads and member tube wall thicknesses is shown in Fig. 12. It demonstrates that there is also a strongly statistically significant trend between LPGA and tube wall thicknesses with a very small variance 0.0455.

Referring to Equation (11), the relationship between lower bound collapse loads and rise to span ratios could be given by:

$$LPGA = 0.0629TH + 3.6977 \pm 0.0455 \quad (15)$$

where $TH \in$ [5.0 mm, 12.5 mm] is the tube wall thickness.

Table. 11
Lower bound collapse loads changing with tube thicknesses

	Tube dimensions: outside diameter (mm)×Wall thickness (mm)		Lower bound collapse load (m/s²)
	Radial and Hoop t_1	Oblique t_2	
A	168.00×5.00	152.00×4.00	51.20
B	168.00×6.00	152.00×4.80	60.50
C	168.00×6.30	152.00×5.04	61.93
D	168.00×8.00	152.00×6.40	70.86
E	168.00×10.00	152.00×8.00	73.56
F	168.00×12.50	152.00×10.0	87.37

Note: t_1:t_2=1:0.8

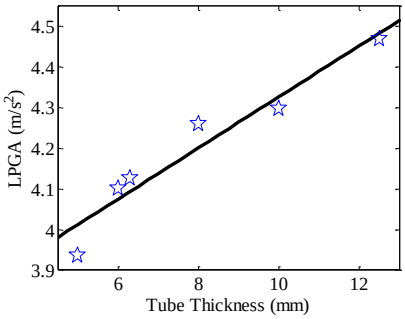

Fig. 12 Relationship between lower bound collapse loads and tube wall thicknesses

4.5 Relationship between lower bound collapse loads and the tube outer diameters

In this section, the dome spans D50065 with tube outer diameters A, B, C, D, E, F, G, H and I (shown in Table 13) were firstly selected as typical cases as shown in Table 12. Then the RHAs were performed in ANSYS software for these typical cases subjected to the twenty seismic records listed in Table 3. The collapse loads for D50065 with different tube outer diameters subjected to twenty seismic records are listed in Table 12, and their collapse fragility curves, lognormal distributions, are shown in Fig. 13.

The lower bound collapse loads with 95% probability of non-exceedance changing with tube outer diameters are also listed in Table 13 based on the collapse fragility curves given in Fig. 13.

On the basis of Table 13, the relationship between logarithmic lower bound collapse loads and logarithmic tube outer diameters is shown in Fig. 14. This demonstrates that there is also a strongly statistically significant trend between LPGA and logarithmic tube outer diameters with a very small variance 0.1645.

The relationship between LPGAs and logarithmic tube outer diameters could be given by:

$$\log(PGA) = 2.3243\log(OD) - 8.0037 \pm 0.1645 \tag{16}$$

where $OD \in$ [114.30 mm, 355.6 mm] is the tube outer diameter, log (OD) is the logarithmic tube outer diameter.

Table 12
The collapse loads for D50065 with different tube outer diameters subjected to twenty seismic records

Number	Collapse loads (m/s²)								
	A	B	C	D	E	F	G	H	I
1	27.60	59.20	127.20	180.80	248.60	306.00	347.40	437.00	450.00
2	27.20	50.60	103.60	140.60	187.60	228.80	254.00	341.60	343.40
3	38.00	73.40	146.00	215.80	269.60	299.80	376.60	486.40	562.20
4	33.20	75.80	140.00	161.20	201.80	262.20	312.00	374.00	445.40
5	24.00	51.60	99.20	149.80	184.60	230.20	270.00	326.00	386.60
6	31.40	67.20	126.60	173.40	243.00	298.40	348.60	490.00	449.00
7	33.40	65.00	120.00	165.60	213.40	259.40	380.60	362.80	485.20
8	30.20	54.60	93.40	121.80	152.20	181.00	211.80	255.40	293.20
9	14.00	27.20	62.40	87.80	116.80	148.60	184.40	270.40	299.40
10	34.80	66.80	113.00	151.80	241.40	239.00	285.00	364.20	386.80
11	29.20	56.80	106.60	143.60	184.60	223.20	278.60	345.80	428.80
12	30.60	65.60	124.60	177.80	245.80	314.20	390.60	485.40	572.00
13	38.60	77.60	159.80	235.00	310.80	395.80	469.00	593.80	681.60
14	32.00	69.00	136.00	195.60	241.40	290.60	346.40	448.80	477.80
15	35.00	70.60	121.00	155.60	193.60	230.40	271.60	346.00	384.40
16	19.20	37.00	71.80	96.60	125.20	154.20	183.40	232.60	273.80
17	15.00	27.60	66.40	93.40	123.00	146.00	180.00	253.00	283.80
18	16.00	30.20	56.40	76.00	95.60	112.20	132.20	169.60	188.60
19	25.80	46.80	90.00	118.00	148.40	186.20	229.00	283.40	307.40
20	15.80	32.00	65.60	90.00	113.80	138.80	171.00	250.20	269.20

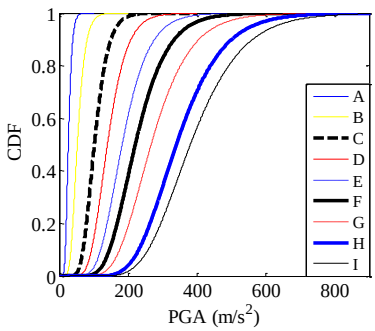

Fig. 13 Collapse fragility curves for D50065 with different tube outer diameters

Table. 13
Lower bound collapse loads changing with tube outer parameters

	Outer parameters (mm×mm)		Lower bound collapse load (m/s²)
	Radial and Hoop D_1	Oblique D_2	
A	114.30×6.30	102.90×5.04	15.60
B	139.70×6.30	125.70×5.04	29.75
C	168.00×6.30	152.00×5.04	61.93
D	193.70×6.30	174.30×5.04	83.60
E	219.10×6.30	197.20×5.04	106.80
F	244.50×6.30	220.05×5.04	129.60
G	273.00×6.30	245.70×5.04	155.60
H	323.90×6.30	291.50×5.04	206.60
I	355.60×6.30	320.00×5.04	230.75

Note: D_1:D_2=1:0.9

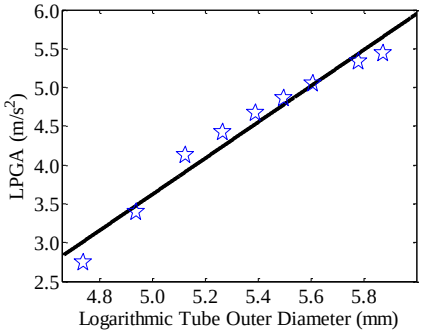

Fig. 14 Relationship between LPGAs and tube outer diameters

4.6 Failure acceleration considering the above key structural design parameters

Based on Eqs. (12) - (16), failure PGA corresponding to the lower bound collapse loads and considering the safety factor in terms of the key structural design parameters is then evaluated as follows.

$$PGA=\frac{1}{1.5}\exp[-0.0090RW-0.0923L+53.5354RSR^3-57.3447RSR^2 +16.4657RSR+0.0629TH+2.3243\log(OD)-4.7194] \quad (17)$$

where $RW \in$ [60 kg, 460 kg] is the roof weight including cladding; $L \in$ [40 m, 90 m] is the structural span; $RSR \in$[0.1, 0.5] is the rise to span ratio; $TH \in$ [5.0 mm, 12.5 mm] is the tube thickness; $OD \in$[114.30 mm, 355.6 mm] is the tube outer diameter.

5. Verification of the fitting formulation and discussion

5.1 Verification

In order to verify the fitting formulation Eq. (17), the domes listed in Table 2 subjected to Taft wave which never participated in obtaining the fitting formulation were selected to compare the failure PGAs. Then, the failure PGAs from different domes calculated separately by using the FEM dynamic response analysis and the fitting formulation Eq. (17) are given in Table 14. Here, PGA_1 denotes the failure PGAs obtained by FEM dynamic response analysis, while PGA_2 the PGAs obtained by the Eq. (17) according to the key structural design parameters.

Table 14
The failure PGAs of nine domes obtained from two methods

Dome	PGA_1 (m/s^2)	PGA_2 (m/s^2)
D40203	12.00	10.81
D40205	17.30	15.01
D40207	16.50	13.72
D50203	43.00	22.35
D50205	64.50	31.03
D50207	57.30	28.37
D60063	48.30	12.40
D60065	64.30	17.22
D60067	52.70	15.75

From Table 14, the failure PGAs, PGA_1, obtained from the FEM dynamic response analysis are all larger than that PGA_2 from the fitting formulation Eq. (17), which proves the rationality of the fitting formulation Eq. (17) based on the key structural design parameters. The reason is that the failure PGAs, PGA_2 corresponding to the lower bound collapse loads, calculated by the fitting formulation Eq. (17) considering the safety factor in terms of the key structural design parameters was obtained from their collapse fragility curves with 95% probability of non-exceedance. While the failure PGAs, PGA_1, from the FEM dynamic response analysis depended solely upon one seismic wave, the TAFT wave. For both cases, the domes with rise to span ratio 1/5 have relatively larger failure PGAs than other rise to span ratios, namely this kind of structure with rise to span ratio 1/5 can resist relatively larger three-dimensional seismic waves comparing with the other cases.

5.2. Discussions on the key structural design parameters

This poses a question about which structural parameter is more efficient for an earthquake resistant structure, such as a large roof weight or small roof weight for domes. (1) Fig. 6 illustrates that the LPGA, roof weight - based fundamental seismic capacity ratio, is a linear decreasing function of structural roof weights. (2) It has the similar tendency that the LPGA decreases linearly depending on the increasing structural span *L* as shown in Fig. 8. (3) As illustrated in Fig. 10 in section 5.3, a dome with rise to span ratio 0.2 would seem superior to a dome with other rise to span ratios subjected to three-dimensional seismic waves. Therefore, it is recommended that a dome with rise to span ratio 0.2 should be considered for the structural design of dome space structures in seismic regions. (4) For the parameter of tube cross section, the failure loads increases following with the increase of tube wall thicknesses and outside diameters as shown in Fig. 12 and Fig. 14. Compare to tube thickness, the outer diameter has higher impact on the structural load bearing capacity, as the LPGA ranges from 3.0 to 6.0 within the tube outer diameter range, while it ranges from 4.0 - 4.5 for the tube wall thickness changes. It is in agreement with the fact that changing the tube outer diameters is more efficient to alter the cross-sectional moment of inertia than changing tube thicknesses, which is a key factor for this type of structure which have to resist substantial bending moments.

6. Conclusion

In this present study a new seismic failure criterion has been developed focusing on domes under seismic loads based on key structural design parameters. The following conclusions are drawn.

(1) In developing the new seismic failure criterion, which has taken into account the functions of five important structural design parameters, roof weights, spans, rise to span ratios, member tube wall thicknesses and tube outside diameters, on the failure loads. Besides the five key structural design parameters, it also considered the influence of the properties of earthquake on failure loads. Hence three hundred three-dimensional seismic records from the database of the COSMOS from seven earthquakes on the basis of the main influential factors of ground motion were selected as input seismic waves to attain the failure fragility curves of the dome structures.

(2) A safety factor 1.5 was introduced to translate the limit load into the design load, which could improve the safety of important large space structures. The reason of the higher safety factor is that the value of the statistical life is significantly higher comparing with the cost of the dome construction, which could increase the safety of the dome structures and reduce the risk of death.

(3) The failure seismic loads estimated by the new seismic failure criterion is the lower bound collapse loads with 95% probability of non-exceeded and considering the safety factor in terms of the five key structural design parameters.

(4) The logarithmic lower bound collapse loads (LPGA) are linear decreasing functions of structural roof weights and span, but increase following with the increase of tube member wall thicknesses and outside diameters within the chosen range. Compare to the tube wall thickness, the outer diameter develops a larger effect on the structural load-bearing capacity. For the rise to span ratio, a cubic curve fits well the relation of the LPGA and the ratios, and a dome with a rise to span ratio 0.2 would seem superior to a dome with other ratios subjected to three-dimensional seismic waves.

(5) Further studies are required for domes with other structure factors, such as membrane action, different configurations, boundary conditions, materials, nodes, connections between members and nodes, geometric imperfection and load distribution.

Acknowledgements

The research work is finished by the financial aid from the NSFC (Grant No. 51508472) and IEC\NSFC\170451- International Exchanges 2017 Cost Share (China). Special thanks to all the staffs in IT services in University of Surrey for providing their many computers.

References

[1] Yu Z. W., Zhi X. D., Fan F. and Chen, L., "Effect of substructures upon failure behavior of steel reticulated domes subjected to the severe earthquake", Thin-Walled Structures, 49, 1160-1170, 2011.
[2] Bai Y., Yang L. and Gong L. F., "Elasto-plastic bearing capacity of four types of single-layer reticulated shell structures under fire hazards", International Journal of Structural Stability and Dynamics, 15(3), 1450051-1-15, 2015.
[3] Liu Y. P., Pan S. J., Leung Simon W. K. and Chan S. L., "Design and construction of long-span single-layer dome structures by direct analysis", HKIE Transactions, 25(1), 29-43, 2018.
[4] Liu C. G. and Li H. J., "A novel method to calculate the dynamic reliability of space structures subjected to multi-dimensional multi-support excitations", International Journal of Space Structures, 25(1), 25-34, 2010.

[5] Zhai X. M. and Wang Y. H., "Modeling and dynamic response of steel reticulated shell under blast loading", Shock and Vibration, 20(1), 19-28, 2013.
[6] Nie G. B., Zhi X. D., Fan F. and Dai J.W., "Seismic performance evaluation of single-layer reticulated dome and its fragility analysis", Journal of Constructional Steel Research, 100, 176-182, 2014.
[7] Kong D. W., Fan F. and Zhi X. D., "Seismic performance of single-layer lattice shells with VF-FPB", International Journal of Steel Structures, 14(4), 901-911, 2014.
[8] Li Y. G., Fan F. and Hong H. P., "Effect of support flexibility on seismic responses of a reticulated dome under spatially correlated and coherent excitations", Thin-Walled Structures, 82, 343-351, 2014.
[9] Fan F., Li Y. G., Zhi X. D. and Li L., "Comparison of seismic response of single-layer reticulated dome under uniform and incoherence three-directional excitations", International Journal of Steel Structures, 14(4), 855-863, 2014.
[10] Ma J. L., Wu C. Q., Zhi X. D. and Fan F., "Prediction of confined blast loading in single-layer lattice shells", Advances in Structural Engineering, 17(7), 1029-1043, 2014.
[11] Ye J. H., Zhang Z. Q. and Chu Y., "Strength failure of spatial reticulated structures under multi-support excitation", Earthquake Engineering and Engineering Vibration, 10(1), 21-36, 2011.
[12] Ye J. H., Zhang Z. Q. and Chu Y., "Strength behavior and collapse of spatial-reticulated structures under multi-support excitation", Science China-Technological Sciences, 54, 1624-1638, 2011.
[13] Liu W. Z. and Ye J. H., "Collapse optimization for domes under earthquake using a genetic simulated annealing algorithm", Journal of Constructional Steel Research, 97, 59-68, 2014.
[14] Zhu N. H. and Ye J. H., "Structural vulnerability of a single-layer dome based on its form", Journal of Engineering Mechanics, 140(1), 112-127, 2014.
[15] Yan R. Z., Chen Z. H., Wang X. D., Xiao X. and Yang Y., "Calculation theory and experimental study of the K6 single-layer reticulated shell", International Journal of Steel Structures, 14(2), 195-212, 2014.
[16] Ma H. H., Fan F., Wen P., Zhang H. and Shen S. Z., "Experimental and numerical studies on a single-layer cylindrical reticulated shell with semi-rigid joints", Thin-Walled Structures, 86, 1-9, 2015.
[17] Yang C., Yu Z. X., Sun Y. P., Zhao L., and Zhao H., "Axial residual capacity of circular concrete-filled steel tube stub columns considering local buckling", Advanced Steel Construction, 14(3), 496-513, 2018.
[18] Zhong J., Zhi X. D. and Fan F., "A dominant vibration mode-based scalar ground motion intensity measure for single-layer reticulated domes", Earthquakes and Structures, 11(2), 245-264, 2016.
[19] Fan F., Wang D. Z., Zhi X. D. and Shen S. Z., "Failure modes of reticulated domes subjected to impact and the judgment", Thin-Walled Structures, 48(2), 143-149, 2010.
[20] Ramalingam R. and Jayachandran S. A., "Postbuckling behavior of flexibly connected single layer steel domes", Journal of Constructional Steel Research, 114, 136-145, 2015.
[21] Bruno L., Sassone M. and Fiammetta V., "Effects of the equivalent geometric nodal imperfections on the stability of single layer grid shells", Engineering Structures, 112, 184-199, 2016.
[22] Yan J. C., Qin F., Cao Z. G., Fan F. and Mo Y. L., "Mechanism of coupled instability of single-layer reticulated domes", Engineering Structures, 114, 158-170, 2016.
[23] Zhi X. D., Fan F. and Shen S. Z., "Failure mechanisms of single-layer reticulated domes subjected to earthquakes", International Association of Shell and Spatial Structures, 48(1), 29-44, 2007.
[24] Yu Z. X., Qiao Y.K., Zhao L., Xu H., Zhao S. C. and Liu Y. P., "A simple analytical method for evaluation of flexible rockfall barrier part 1: working mechanism and analytical solution", Advanced Steel Construction, 14(2), 115-141.
[25] Standardization Administration of China, Technical specification for space frame structures, JGJ 7 -2010, Beijing, China Architecture & Building Press, 2010. (in Chinese).
[26] Architectural Institute of Japan, Dynamic Behavior and Seismic Design of Spatial Structures, Tokyo, Showa Joho Process, 2006.
[27] American Institute of Steel Construction, Seismic Provisions for Structural Steel Buildings, ANSI/AISC 341-10, Chicago, 2010.
[28] British Standards Institution, Eurocode 8: Design of Structures for Earthquake Resistance – Part 1: General Rules, Seismic Actions and Rules for Buildings, CEN. EN 1998-1, 2004.
[29] ANSYS 10.0. Theory reference. ANSYS Inc. 2005.
[30] Vamvatsikos D, Cornel CA, "Incremental dynamic analysis", Earthquake Engineering and Structural Dynamics, 31(3), 491-514, 2002.
[31] COSMOS Virtual Data Center. (http:/db.cosmos-eq.erg/scripts/default.plx).
[32] Johnson Norman L., Kotz Samuel, Balakrishnan N., "14: Lognormal Distributions", Continuous univariate distributions, Vol. 1, Wiley Series in Probability and Mathematical Statistics: Applied Probability and Statistics (2nd ed.), New York: John Wiley & Sons, ISBN978-0-471-58495-7,MR1299979, 1994.
[33] Papoulis A. P., Pillai S. U., "Probability, Random Variables, and Stochastic Processes (4th ed.)". Boston, McGraw-Hill, ISBN 0-07-366011-6, 2002.
[34] http://ocw.mit.edu/courses/mathematics/18-443- statistics -for-applications-fall-2006/lecture-notes/lecture6. pdf.
[35] Benjamin J. R., Cornell C. A., "Probability, Statistics, and Decision for Civil Engineers", McGraw-Hill: New York, NY, 1970; 684.
[36] Soutsos M. N., Breysse D., Garnier V., Goncalves A. and Monteiro A. V., "Estimation of on-site compressive strength of concrete", In Non-Destructive Assessment of Concrete Structures, Reliability and Limits of Single and Combined Techniques, RILEM, Talence, France, 2012.
[37] American Institute of Steel Construction, Specification for Structural Steel Buildings, ANSI/AISC 360-16, Chicago, 2016.
[38] Department of Transportation, Standard Specifications, CalTrans, State of California, 2015.
[39] Department of Defense, J Joint service specification guide: Aircraft structures, SSG – 2006, Washington, U.S, 1998 .
[40] Department of the Prime Minister and Cabinet, Best Practice Regulation Guidance Note: Value of statistical life, Australian Government, 2014.
[41] Ministry of Transport, Social cost of road crashes and injuries 2016 update, New Zealand Government, 2016.
[42] Department of Transportation, Guidance on Treatment of the economic value of a statistical life (VSL) in U.S. department of transportation analyses-2016 adjustment, Office of the Secretary of Transportation, U. S., 2016.
[43] Shen S. Z., Zhi X. D., "Failure mechanism of reticular shells subjected to dynamic actions", the 4th International Conference for Advances in Steel Structures, ShangHai, China, 2005.
[44] Ibarra LF, Krawinkler H, "Global collapse of frame structures under seismic excitations", Report No. 152, The John A. Blume Earthquake Engineering Center, Department of Civil and Environmental Engineering, Stanford University, Stanford, CA, 2005.
[45] Zhong J., "Probabilistic Seismic Fragility Analysis of Reticulated Shells", PhD thesis, Harbin Institute of Technology, Harbin, China, 2016. (in Chinese).
[46] Fan F., Zhi X. D. and Shen S. Z., "Failure mechanism of reticulated shells under earthquake", Science Press, 2014. (in Chinese).

Appendix Table 1. The domes with various structural parameters

	Span (m)	Roof weight (kg/m^2)	Ratio of rise-span	Cross section (mm)	
				radial and hoop members	oblique members
Domes with various roof weights	50	60	0.20	168.00×6.00	152.00×5.00
		100			
		160			
		200			
		260			
		300			
		360			
		400			
		460			
Domes with various spans	40	60	0.20	168.00×6.00	152.00×5.00
	50				
	60				
	65				
	70				
	75				
	80				
	85				
	90				
Domes with various rise to span ratios	50	60	0.10	168.00×6.00	152.00×5.00
			0.15		
			0.20		
			0.25		
			0.30		
			0.35		
			0.40		
			0.45		
			0.50		
Domes with various tube thicknesses	50	60	0.20	168.00×5.00	152.00×4.00
				168.00×6.00	152.00×4.80
				168.00×6.30	152.00×5.04
				168.00×8.00	152.00×6.40
				168.00×10.00	152.00×8.00
				168.00×12.50	152.00×10.00
Domes with various tube outside diameters	50	60	0.2	114.30×6.30	102.90×5.04
				139.70×6.30	125.70×5.04
				168.00×6.30	152.00×5.04
				193.70×6.30	174.30×5.04
				219.10×6.30	197.20×5.04
				244.50×6.30	220.05×5.04
				273.00×6.30	245.70×5.04
				323.90×6.30	291.50×5.04
				355.60×6.30	320.00×5.04